Journal of Power Sources 196 (2011) 9398–9406

Contents lists available at ScienceDirect

Journal of Power Sources

journal homepage: www.elsevier.com/locate/jpowsour

Battery parameter identification with Pseudo Random Binary Sequence excitation (PRBS)

A.J. Fairweather[a,*], M.P. Foster[b], D.A. Stone[b]

[a] VxI Power Ltd, Station Road, North Hykeham, Lincoln, LN6 3QY, UK
[b] Department of Electrical and Electronic Engineering, The University of Sheffield, UK

ARTICLE INFO

Article history:
Received 30 April 2011
Accepted 22 June 2011
Available online 8 July 2011

Keywords:
Batteries
Modelling
PRBS
State estimation

ABSTRACT

This paper extends previous work on the use of maximum length sequences as tools for parameter estimation within electrochemical batteries. An improved technique using a simplified monopolar current pulse excitation strategy allows identification of Randles' model equivalent circuit values, which can be subsequently employed in state-of-charge and state-of-health algorithms. Within the approach the problems associated with establishing bulk capacitance over a short time period are avoided. Instead, using readily identifiable parameters (surface capacitance, series resistance and charge transfer resistance) comparison of parameters for new and aged batteries is carried out, and a potential indicator for State of Health described. Experimental results are presented to verify the proposed technique.

1. Introduction

The growth in portable electronic devices, the incentives of renewable energy usage, and the increasing use of electric vehicles is leading to new applications for batteries. As these new applications emerge greater importance is placed on knowing the available capacity of a battery, termed the State of Charge (SoC), and a measure of the battery's health, State of Health (SoH), one such measure being the battery's present capacity compared to its on-the-shelf capacity. The knowledge of the current SoC and SoH of a battery is becoming increasingly important in many applications, such as electric vehicles and Uninterruptable Power Supplies (UPS), since it is the battery state that ultimately dictates the performance of the whole system.

To date Coulomb counting is the most common method for measuring state-of-charge since it involves simple current integration [1]. However, a disadvantage of this technique is that a periodic recalibration process is required due to the cumulative errors that can occur when small measurements are integrated over a long period of time, and a recalibration of the total battery capacity is also required to allow the total charge counted to be equated to battery SoC. In practice the recalibration process may require a complete discharge and recharge cycle which can be impractical for systems where batteries are regularly recharged from a partially discharged state, or where the batteries may be connected in an unknown state to the host system charger. Multiple input charge systems, such as renewable energy mini grids, may have several sources of charge (solar photovoltaic and wind turbines) operating at differing rates, with a variable load, making a Coulomb counting system complex to implement. Current pulse impedance spectroscopy has been successfully applied but requires the battery to be disconnected from its load, or the load to be placed in a known state, which may interfere with normal system operation [2–4] and spectroscopy test time is dependent on battery capacity, which can be large depending on the application. Other techniques which employ state-observers [5] have been reported but they often require specialist control systems knowledge impeding their adoption by industry. This paper presents a parameter identification technique employing Pseudo Random Binary Sequence (PRBS) current pulse excitation that can be applied online to provide estimates for Randles' equivalent circuit, which offers a reduction in test time of several orders of magnitude, and removes the requirement for recalibration or load/charger disconnection.

Previous work using PRBS [6] has considered the overall battery impedance over varying states of charge. This paper expands this work into analysis of the individual circuit components themselves in order that characteristics can be identified to describe the overall battery condition.

Lead Acid batteries remain the dominant battery chemistry for automotive applications, renewable energy, and UPS applications, despite not being the highest energy density, they offer the lowest cost/capacity and have a recycling infrastructure which is mature and efficient.

The work described in this paper was undertaken using Valve Regulated Lead Acid (VRLA) batteries manufactured by Yuasa

* Corresponding author. Tel.: +44 1522500511; fax: +44 1522500515.
E-mail addresses: andrew.fairweather@vxipower.com (A.J. Fairweather), m.p.foster@sheffield.ac.uk (M.P. Foster), D.A.Stone@sheffield.ac.uk (D.A. Stone).

0378-7753/$ – see front matter © 2011 Published by Elsevier B.V.
doi:10.1016/j.jpowsour.2011.06.072

Nomenclature

Δt	PRBS clock period, s
c	Rated capacity, Ah
C	Capacitance, F
C_{bulk}	Bulk capacitive element of cell, F
C_p	Peukert capacity, Ah
$C_{surface}$	Double layer capacitance, F
f_{band}	PRBS bandwidth, Hz
f_c	PRBS clock frequency, Hz
f_{max}	maximum frequency in PRBS bandwidth, Hz
f_{min}	minimum frequency in PRBS bandwidth, Hz
f_{norm}	Normalised PRBS bandwidth, Hz
I	Current, A
K	Peukert coefficient
n	PRBS bits
N	PRBS sequence length
R_d	Self discharge resistance, Ω
R_i	Series resistive element (Randle's circuit), Ω
R_t	Charge transfer resistance, Ω
T	time, s
V_{EOD}	End of discharge voltage, V
V_{OCT}	Open circuit terminal voltage, V
$W_{C_{bulk}}$	Energy stored within bulk capacitor, J
τ	Time constant, s

(65 Ah, 12 V batteries); however, the principles and techniques are widely applicable to a range of chemistries. The tests were carried out using fully charged batteries, the work being focused on indicators of SoH in the first instance. One new battery and one aged battery were used for comparative tests, in order that the advantages of the PRBS technique could be shown, and these indicators presented.

The remainder of the paper is organised as follows. Section 2 discusses battery models and their application, Section 3 describes experiments using conventional techniques to establish the equivalent circuit components for the batteries under test. Section 4 examines the design of the PRBS sequence and constraints on its use. Section 5 examines the battery equivalent circuit based on the parameters established in Section 3, in order to predict likely outcomes, and also informs the PRBS analysis carried out later.

Section 6 presents experimental results obtained from the PRBS identification technique, and discusses the parameters obtained. Section 7 draws conclusions from the preceding work and offers suggestions for further study.

2. Battery models

Parameter estimation for any system requires that a suitable model be established. In the analysis of batteries, several models are in widespread use, and are borrowed from their usage in analysis of electrochemical cells which may not specifically be electrical storage devices, example applications ranging from DNA analysis [7] to modelling of reinforced concrete corrosion [8].

In the general approach to battery models an *R–C* linear equivalent circuit model is employed, which in its most simplistic form, comprises a capacitor, representing the bulk energy store, and series resistor. This model, however, is limited in use, as it in no way truly represents any of the chemical processes. It therefore follows that an improved model, with representation of the predominant chemical phenomena, should be used as the basis for further evolution of the described system. Detailed models have been developed for secondary cells using these processes [9], which generally evolve from the familiar Randles' model [10]

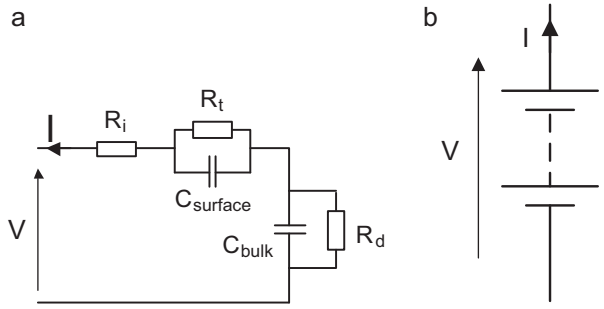

Fig. 1. Randles' equivalent circuit (a) and battery showing terminal voltage and discharge current (b).

which is used for the work described in this paper. The model is a straightforward electrical representation of the complex electrochemical processes, with lumped parameters representing the cell. The model assumes the cell behaviour under both charge and discharge conditions are identical, and charge transfer is achieved with 100% efficiency.

Considering Randles' model (Fig. 1) R_i is the lumped resistance for the cell interconnections, etc. and represents the major series resistance for the cell. $C_{surface}$ is a double layer capacitance, which is a result of the charge separation at the interface between the electrolyte and the cell plate [11]. The resistor, R_t, that is connected in parallel with the double layer capacitance is the charge transfer resistance and is the electrical analogy of the inherent speed of the charge transfer reaction.

C_{bulk} represents the dominant capacitive element of the cell and R_d is the self discharge resistance of the cell, shown as a load connected across the bulk element of capacitance. R_d is typically high for a healthy cell, and is most commonly quoted by the manufacturer in terms of a percentage discharge per month. Yuasa provide a figure of 3% per month self discharge at 20 °C for the NP battery range, which translates into a value for R_d of approximately 5 kΩ, for the 65 Ah batteries used in the experiments [12].

3. Cell parameter estimation using conventional methods

Analysis of cells, and batteries, by conventional means is well understood, and a number of methods can be employed to examine the equivalent circuit components. In order to validate the results of the PRBS testing, it was necessary first to establish the equivalent circuit parameters using conventional tests employing step load pulses, and controlled constant-current discharges.

3.1. Determination of C_{bulk}

Establishing the overall capacity, and from that the bulk capacitance, requires the removal of usable energy from the battery. This is achieved by discharging a fully charged battery into a known load, and monitoring the battery's electrical characteristics.

For a given discharge rate, manufacturers data will state the minimum end-of-discharge voltage (V_{EOD}) for a particular battery. Beyond this point irreversible capacity loss will occur, and the battery will be permanently damaged. The majority of VRLA batteries are rated at a 20 h discharge rate, usually quoted as a factor of overall capacity, i.e. 0.05 c for 20 h.

Typically for this discharge rate, with a 20 °C battery temperature, V_{EOD} will be around 1.75 V/cell [12] (10.5 V for a 6 cell, 12 V battery). Therefore, initial estimates of the capacitance of a battery can be made before verification by experiment, based on estimated initial open-circuit-terminal (V_{OCT}) and end (V_{EOD}) voltages. Discharging the battery then provides the actual battery capacity,

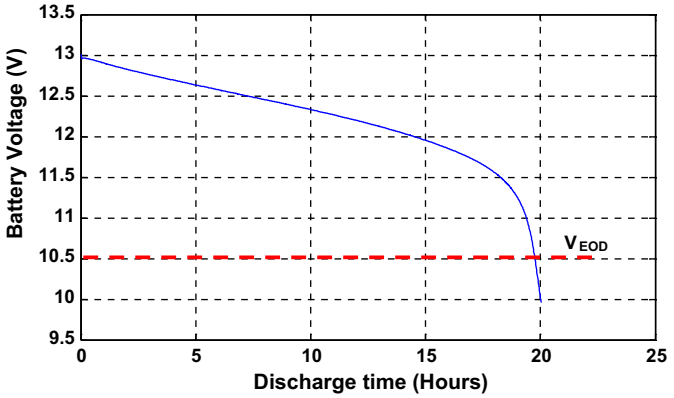

Fig. 2. Typical discharge curve for a VRLA battery showing usable energy.

which requires a measurement of discharge time to V_{EOD} from the steady state V_{OCT} allowing the energy to be determined (Fig. 2).

Prior to the capacity discharge test the batteries were charged at a constant voltage, using a temperature compensated battery charger. The batteries were then left for a period of 4–6 h in an open circuit condition in order to establish a stable off-charge terminal voltage (V_{OCT}).

A discharge test was performed, corresponding to the 20 h discharge rate, (0.05 c) and the batteries discharged. Fig. 3 shows the discharge profile for the batteries. At the start of the discharge V_{OCT} is around 12.8 V, falling to V_{EOD} at 10.5 V.

The capacity in Ah is calculated, from which the energy transferred from the battery to the load, $W_{C_{bulk}}$, can be determined. A value for the bulk capacitor is obtained by equating from the capacitor energy equation.

$$W_{C_{bulk}} = \frac{1}{2}C_{bulk}(V^2) \quad (1)$$

$$= \frac{1}{2}C_{bulk}(V^2 - V^2) \quad (2)$$

And therefore,

$$C_{bulk\ initial} = \frac{\text{Rated capacity}\, x V_{oct}}{1/2(V_{OCT}^2 - V_{EOD}^2)} \quad (3)$$

Analysis of the discharge curves for the new and aged batteries revealed a difference in capacity of 7%.

Therefore further tests were carried out to establish the variation in C_{bulk} with increased discharge. Peukert's equation [13] describes how Lead Acid cells and batteries vary in available capacity for different rates of discharge.

$$C_p = I^k t \quad (4)$$

where C_p is capacity according to Peukert, at a specified discharge rate.

I is discharge current in Amperes; k is the Peukert constant for the battery; t is the time of discharge in hours.

Representative curves are provided in the manufacturer's data based on Peukert's equation [12] and therefore these further tests were used to establish if the aged battery showed any further loss of capacity with increased discharge rate. The batteries were subjected to $c/4$, $c/2$ and 1c discharges, and the results from the discharge tests for both batteries can be seen in Fig. 4. With increased discharge rates deviations from expected performance were observed. For the higher rate discharge tests capacity differences between the two batteries increased, rising to around 20% for the 1c test on the aged battery, with a characteristic steep fall in terminal voltage seen on application of the load. This further indicated the degrading SoH of the aged battery and possible trends towards ends of life.

3.2. Determination of $C_{surface}$, R_i, R_t

The evaluation of $C_{surface}$ requires a slightly different approach to that of C_{bulk} in that $C_{surface}$ is most apparent during transient conditions in discharge to off-load situations. As such this excitation must be designed, and it is important that the method employed is not affected by C_{bulk}. Previous work [14] has shown that the time constant associated with C_{bulk} is very much larger than that associated with $C_{surface}$, and therefore pulse testing can be used to excite the dynamics associated with $C_{surface}$ without significantly affecting C_{bulk}, typical pulse widths of 500 mS (2 Hz) have been quoted [5].

From a fully charged state, a constant current discharge of 8A was applied to the battery, and during this period, short interruptions to the load were made in order to observe the transient terminal voltage of the batteries. Fig. 5 shows the terminal voltage of the battery during the test, at100% SoC.

With reference to Fig. 5, the battery is initially discharging at a constant current, and the terminal voltage is considered to be in a time-limited pseudo steady-state and thus, one may assume, at this

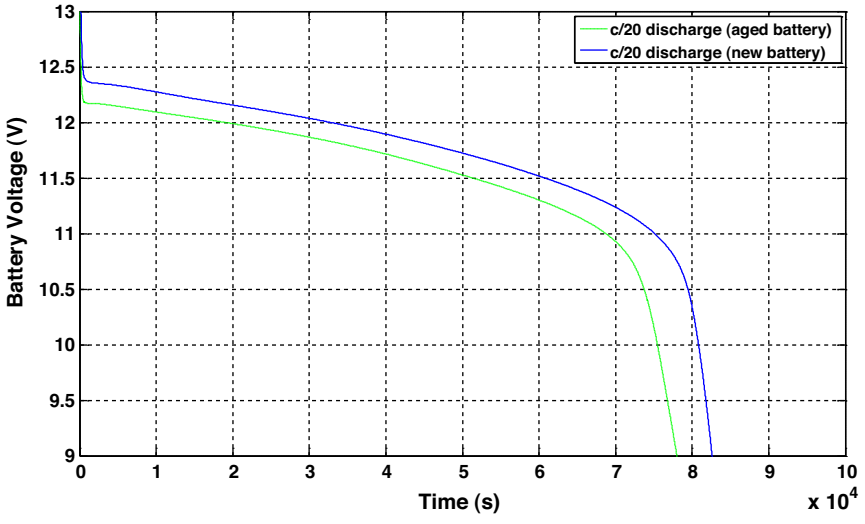

Fig. 3. Actual discharge curves for the batteries tested, $c/20$ discharge rate.

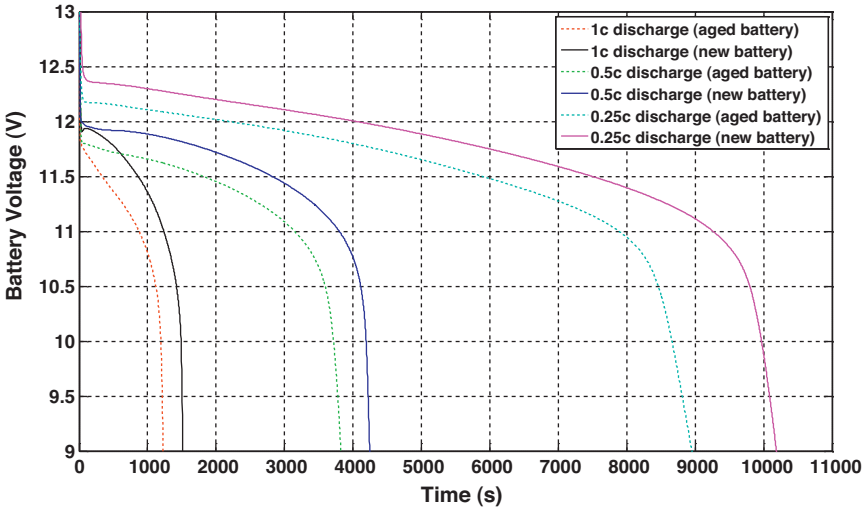

Fig. 4. Discharge curves for the test batteries at increased discharge rates of $c/4$, $c/2$ and $1c$.

Table 1
Parameters obtained from the test batteries using the pulse tests.

New battery	Aged battery
V_{OCT} = 12.846 V	V_{OCT} = 12.807 V
V_{EOD} = 10.5 V	V_{EOD} = 10.5 V
Ampere second capacity = 259992 As	Ampere second capacity = 241839 As
C_{bulk} = 121960 F	C_{bulk} = 115205 F
$C_{surface}$ = 14.81 F	$C_{surface}$ = 5.59 F
R_i = 5.08m Ω	R_i = 5.6 mΩ
R_t = 5.18m Ω	R_t = 6.5 mΩ
R_d = 5034 Ω	R_d = 4955 Ω

point that the decay in terminal voltage is completely attributable to the discharge of the bulk capacitor. As the load is removed, a step change in terminal voltage occurs, which is predominantly attributable to the series impedance, R_i. Following the step change $C_{surface}$ begins to charge (previously discharged during the load period). The load is re applied, and again the effect of R_i is seen, followed by the discharge of $C_{surface}$. As previously discussed the value of $C_{surface}$ is several orders of magnitude smaller than C_{bulk} allowing a reasonable degree of clarity regarding measuring the time constant, without introducing any significant error due to the discharge of C_{bulk} itself.

From the responses obtained, the equations below were used to obtain the parameters of interest, shown in Table 1.

$$R_i = \frac{\Delta V_1}{I} \tag{5}$$

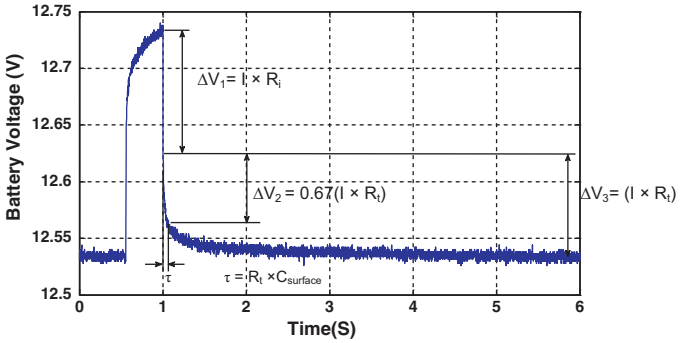

Fig. 5. Calculation of model parameters.

$$R_t = \frac{0.671}{\Delta V_2} \tag{6}$$

$$C_{surface} = \frac{\tau}{R_t} \tag{7}$$

3.3. Determination of R_d

For a battery approaching end of life, the value of R_d may decrease, and must also be considered in this calculation. Decay of V_{OCT} for a fully charged battery should be monitored to identify the value of R_d. The test batteries were fully charged and connected to a data acquisition system of sufficiently high input impedance (>100 KΩ) as not to effect the self discharge caused by R_d. The decay in terminal voltage was measured over several weeks in order that the value of R_d could therefore be calculated.

4. Pseudo Random Binary Sequence (PRBS) parameter identification

One major disadvantage of the characterisation procedure described in Section 3 is that three separate tests were required to extract parameters for the Randles' model and each of these tests required specialised test equipment. By contrast frequency domain characterisation allows the parameters to be extracted using just one item of test equipment. Additionally, batteries and cells do contain complex electrochemical reactions, which are most often sought to be modelled by Electrical Engineers. The frequency domain approach with electrical analogues does therefore lead to a more straightforward understanding of the modelling process.

Analysis of systems in the frequency domain requires a suitable excitation signal and the use of random signals to establish a frequency response is becoming a widespread alternative to swept sine techniques which are sometimes laborious and cumbersome. Choice of perturbation signal is often driven by the type of system to be identified and the desired method of signal processing, with an approximation to white noise being the goal. Signals generated digitally, that can offer this are attractive, since with the widespread availability of low cost embedded digital signal processors, the acquisition, excitation and analysis can be realised within a single device.

PRBS or maximum length sequences (MLS) find applications over many disciplines for parameter identification since the frequency spectrum of the PRBS is known to approximate to band-

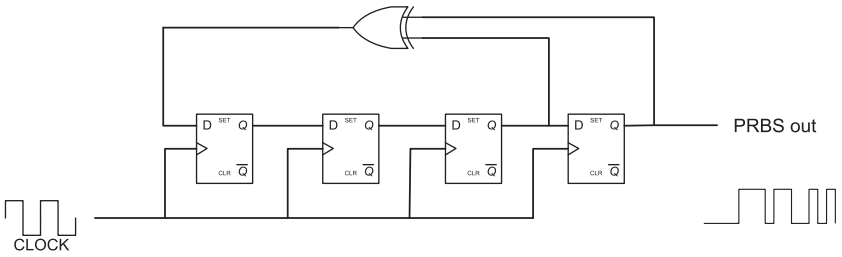

Fig. 6. 4-bit PRBS generator example.

limited white noise, and thus they form a useful stimulus for frequency response analysis. The stimulus signal can be injected in isolation, or in addition to the usual input/control signal, and the output response measured. Fourier analysis techniques can then be employed to determine the system's frequency response. Applications of this technique include hearing aid analysis [15], impedance spectroscopy [16], and switched mode power supply control loop analysis [17].

4.1. Characteristics and design of PRBS

The use of PRBS in frequency domain analysis requires, as with any bandwidth limited perturbation signal, correct design of the signal parameters themselves in order that the frequencies of interest can be examined. PRBS generators can be realised by shift registers with modulo 2 (XOR) feedback at predetermined "tap" positions [18]. Fig. 6 provides an example of a 4-bit PRBS generator.

Alternatively, within an embedded software environment, a look up table for the sequence may be used. The number of stages, n, defines the number of terms, N in the sequence. Considering that all states apart from "all zeros" are represented,

$$N = (2^n - 1) \tag{8}$$

This gives rise to a sequence which repeats every N terms (Fig. 7), as can be seen by the repetitive nature of the autocorrelation function. In Fig. 7 it is assumed that the PRBS has an amplitude of $\pm a$ and is clocked every Δt seconds.

4.2. Limitations of bandwidth for the PRBS

The power spectrum of a PRBS (Fig. 8) consists of discrete frequencies with a magnitude envelope described by the sinc(x) function and the magnitude reaches its first value of zero at the clock frequency [18]. It therefore follows that the PRBS is bandwidth limited at a frequency less than that of the clock. Additionally, the minimum frequency step is defined by the number of terms in the sequence (N) and the duration of the clock pulse (Δt). If one then considers that the Wiener–Khintchine theorem states that the power spectral density of a wide sense stationary random process is the Fourier transform of the corresponding autocorrelation function, it can be shown that PRBS has a usable frequency range of 1/3 of the clock frequency [18].

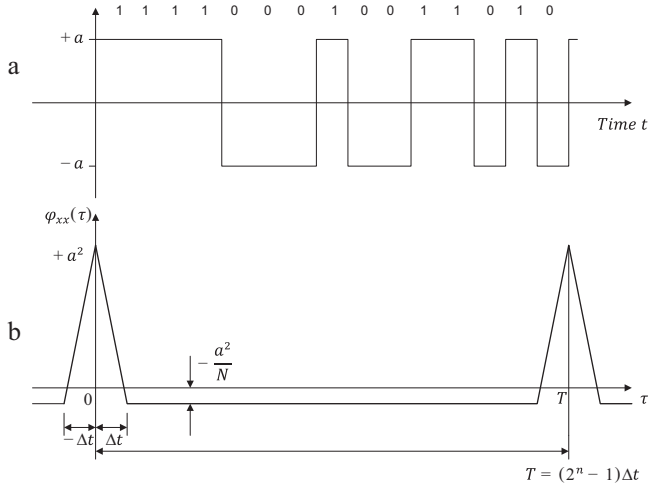

Fig. 7. (a) Example PRBS sequence and (b)typical autocorrelation response.

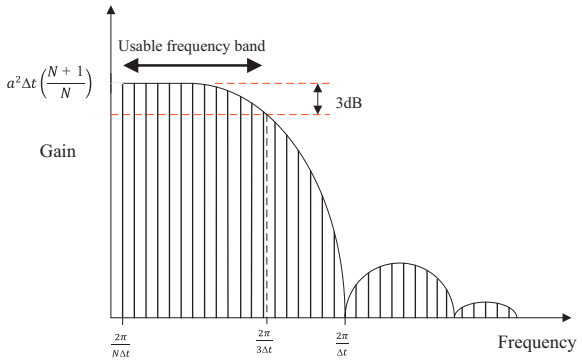

Fig. 8. Power spectrum (FFT) of a PRBS showing usable frequency band.

The two base design parameters for the PRBS are therefore the fundamental clock pulse frequency and the number of stages of the generator itself. Considering the defined band above, the clock frequency, as a general rule of thumb should be chosen to be approximately:

$$f_c = 2.5 f_{max} \tag{9}$$

where f_{max} is the maximum frequency of interest.[19]

4.3. Data acquisition and sampling rate

The usable bandwidth of the PRBS has already been discussed and it therefore follows that the PRBS must be acquired and processed as a complete sequence to maintain its white-noise-like properties. This leads to the consideration of the duration of the test itself, as the PRBS sequence duration (T) will define the amount of data which needs to be acquired. This can lead to very long test times if a PRBS is chosen which has a large number of stages (i.e., a "16 bit" sequence has 65535 terms, and if the frequency of interest is in the Hz range, the time required to capture a valid data sample will be large).

Therefore design of the PRBS should consider usable bandwidth, frequency of interest and the resulting test duration.

As the bit length of the PRBS increases there are diminishing returns with the increase in usable bandwidth. The disadvantage of the use of excessively long sequences can therefore be seen with the increase in required test duration to capture a complete sequence.

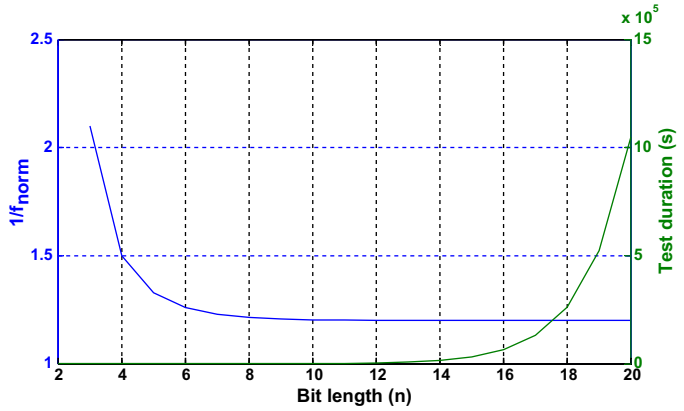

Fig. 9. Normalised bandwidth for length with test duration on same axes.

Sampling rate is dictated by f_c and as the normal requirements of the Nyquist–Shannon sampling theorem must be met, a sampling rate of 2–5 times f_c must be used.

Collecting the terms discussed in describing the bandwidth of the PRBS, allows a normalised bandwidth to be established.

$$f_{\min} = \frac{1}{N\Delta t}, f_{\max} = \frac{1}{3\Delta t}, f_c = 2.5 f_{\max} = \frac{1}{\Delta t} \tag{10}$$

$$f_{\text{band}} = \frac{1}{\Delta t}\left(\frac{1}{3} - \frac{1}{N}\right) = 2.5 f_{\max}\left(\frac{1}{3} - \frac{1}{N}\right) \tag{11}$$

$$f_{\text{norm}} = \frac{f_{\text{band}}}{f_{\max}} = 2.5\left(\frac{1}{3} - \frac{1}{N}\right) \tag{12}$$

The relationship between the parameters is shown in Fig. 9.

Fig. 9 shows the tradeoffs in the PRBS design, as bit length increases, normalised bandwidth (inverted on primary Y axis to emphasise the relationship) increases exponentially. However, with increased bit length the increase in test time becomes a disadvantage. It therefore follows that for low frequency tests, where test time is an issue, the chosen bit length should tend towards the flattest area of the plots in Fig. 9, (e.g. between $n = 8$ and $n = 14$).

4.4. PRBS perturbation signal for experimental battery testing

For the work presented here the battery terminal current was chosen as the perturbation input signal since it is a variable that is more readily controlled, and the battery terminal voltage was designated the perturbation output signal thus allowing the battery's impedance response to be determined.

Since the battery can both sink and source current the perturbation signal needs to be carefully designed so that the change in stored energy is minimised during the characterisation test such to not adversely affect the results. Although the requirement is more readily achieved using a bi-polar current source the authors adopted a mono-polar current sink for this work since this technique can be used over varying SoC. At 100% SoC a current source would tend to overcharge the battery, and the voltage amplitude required to develop the required current signal may push the battery outside of its operational envelope. Using a current sink clearly tends to discharge the battery, thus this led to a trade off between the signal amplitude used and the effect on the SoC such that the sensitivity of the measurements were maximised without adversely affecting the SoC of the battery.

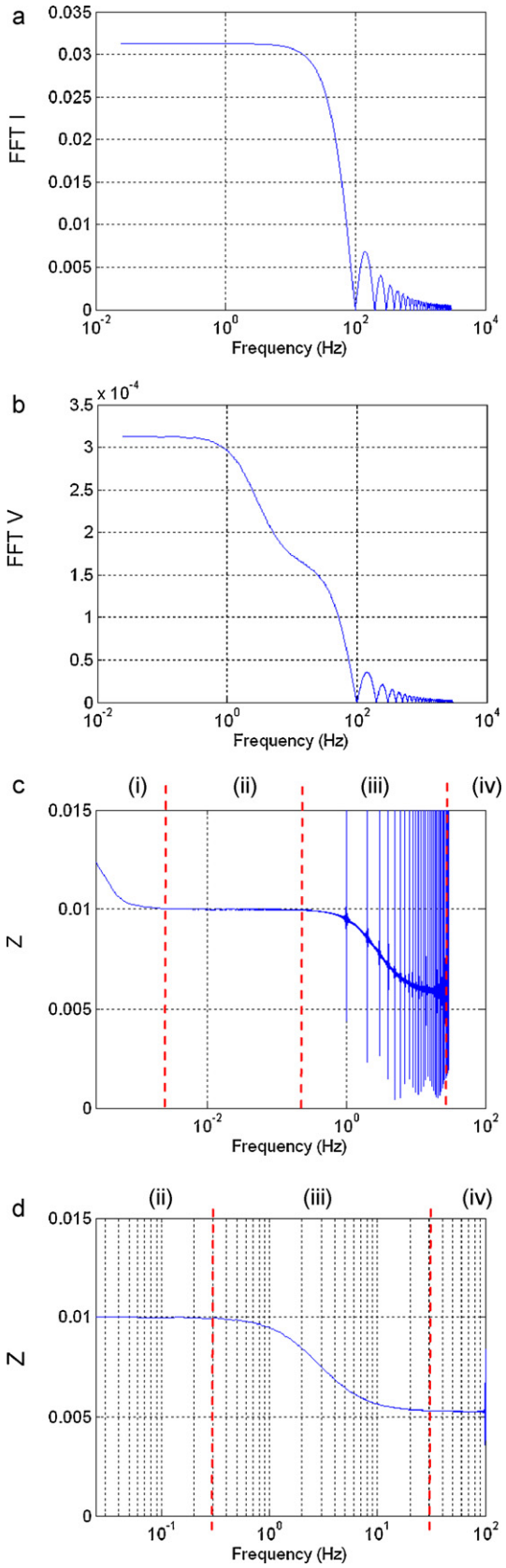

Fig. 10. Impedance responses obtained using conventional test parameters (a) input current FFT, (b) battery terminal voltage FFT, (c) impedance plot with low frequency clock showing bulk capacitor response. (d) Impedance plot with higher speed clock showing more detail for C_{surface} and R_i.

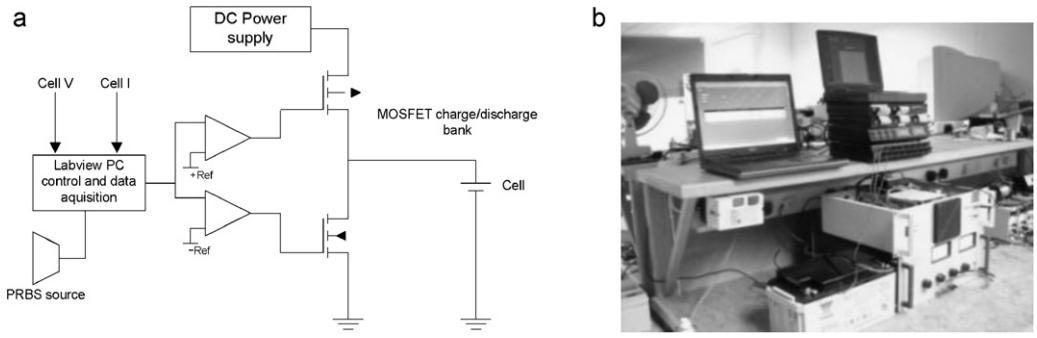

Fig. 11. (a) Test system block diagram and (b) photograph of test rig.

5. Examination of battery impedance

The parameters obtained from the conventional tests (Table 1) allowed an examination of the impedance response for the battery using computational techniques. The results of this approach were used to inform the PRBS design process, for the later experimental analysis.

5.1. Sampled data model analysis

In order to obtain plots for battery impedance based on the results of conventional tests, a sampled data model was created in Matlab. The PRBS sequence was generated and applied to the Randles' model, with values for the equivalent circuit established earlier. FFTs of both the input current waveform and the corresponding battery terminal voltage were evaluated. From these spectra an output characteristic could then be obtained, as shown in Fig. 10.

At lower frequencies, section (i) of Fig. 10(c), a gradient due to C_{bulk} is observed. In considering the plateau in the centre of the response (ii) the sum of $R_i + R_t$ is presented. Beyond this plateau, (iii) C_{surface} becomes dominant before the curve finally becomes asymptotic to R_i (iv) as the response becomes purely resistive with increasing frequency.

It follows that this analysis gives rise to the following set of equations, respectively:

$$Z_1 = \frac{1}{\sqrt{(1/R_d{}^2 + 1/x_{c_{bulk}}{}^2)}} + \frac{1}{\sqrt{(1/R_t{}^2 + 1/x_{c_{surface}}{}^2)}} + R_i + R_t \quad (13)$$

$$Z_2 = R_i + R_t \quad (14)$$

$$Z_3 = \frac{1}{\sqrt{(1/R_t{}^2 + 1/x_{c_{surface}}{}^2)}} \quad (15)$$

$$Z_4 = R_i \quad (16)$$

6. Experimental PRBS investigation – test system description

A high-power battery cell characterisation apparatus, Fig. 11, was developed featuring data acquisition, high-bandwidth current amplifier and PRBS generator. The overall control was provided by the PC based National Instruments LabVIEW control system, with PRBS signal input provided by an external embedded processor, allowing fast implementation of the input signal, outside of the computational overhead of the PC environment. A bank of parallel connected MOSFETs provide current sink to the battery under test. Closed loop analogue control of the MOSFET bank provided rapid operation and close control over the transient response which allows drive by the PRBS to be replicated with minimal settling time and reduced rise/fall times. On board high bandwidth current measurement is provided for, with data acquisition integral to the system, allowing data analysis to be performed off-line. Initial charge is provided by a closely controlled battery charger manufactured by VxI Power Ltd. The charger incorporates a microcontroller managed charging regime with temperature compensation. Periodic terminal voltage measurements during charging are inherent to the VxI unit, allowing an assessment to be made of the battery's ability to accept charge, and to highlight excessive self discharge.

6.1. Test procedure

The battery was fully charged, and allowed to establish a steady-state terminal voltage before the tests were carried out. The current pulse amplitude was selected in order to provide good signal to noise ratio, without producing a significant discharge.

The excitation signal was applied to the test system using a dsPIC development board, running a simple routine written in C. The PRBS

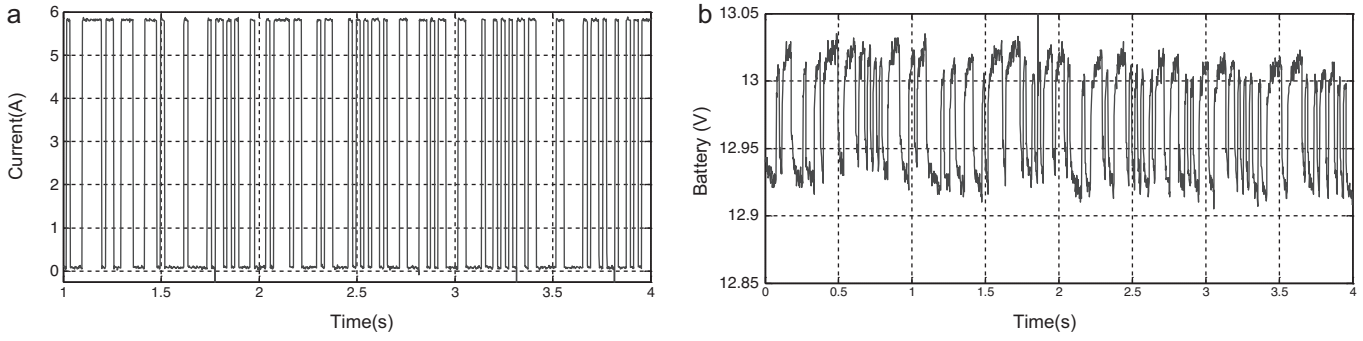

Fig. 12. (a) Excerpt from acquired PRBS current perturbation and (b) battery voltage during test.

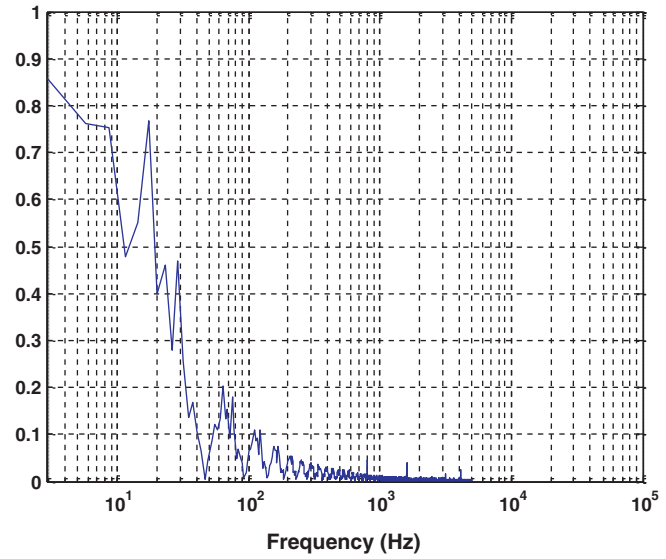

Fig. 13. FFT of battery terminal voltage during test.

sequence was held in memory, rather than being generated by shift registers, to minimise timing errors. For minimum test time a low order bit sequence was used, the tradeoffs being a reduction in bandwidth and resolution.

In the literature it is well acknowledged, [18–20] that to minimise the effects of spectral leakage and other artefacts complete PRBS sequences must be processed. The authors can further verify since during off line processing, the capture of non-exact multiples of T gave rise to considerable signal spectral content degradation. Correspondingly analysis routines written in Matlab extracted exact sequences of acquired data to be processed.

6.2. Results

Fig. 12(a) shows an example of the PRBS current perturbation signal, and the resultant battery terminal voltage, (b). An example FFT is shown, Fig. 13

For these experiments, the values of R_i, R_t and $C_{surface}$ were determined. R_i is used by simple battery testing schemes as an indicator of SoH [3]. Examination of other previous work had also indicated these parameters as good indicators of SoH [5].

The values for R_i, R_t and $C_{surface}$ can be obtained directly by inspection or by calculation. Considering points on the response, multiple impedances present themselves corresponding to the components at these frequencies, which will be directly influenced by $C_{surface}$ itself.

Considering responses plotted earlier (Fig. 10,) the response tends to R_i at high frequency. Moving towards the lower frequencies the effect of $C_{surface}$ decreases and the impedance of the parallel combination of $C_{surface}$ and R_t becomes significant. This impedance is:

$$Z(\omega) = \frac{1}{\sqrt{(1/{R_t}^2 + (\omega C_{surface})^2)}} \tag{17}$$

Calculating a value for $C_{surface}$ without R_t can be carried out by taking more than one point from the response, and solving simultaneous equations at frequencies ω_1 and ω_2. R_i must be taken into account however, and as already mentioned, the response tends to R_i at high frequency. (Fig. 14(b)).

Therefore, if Z_{t1} and Z_{t2} are two points on the characteristic response for $C_{surface}$ and R_t, at frequencies ω_1 and ω_2 respectively,

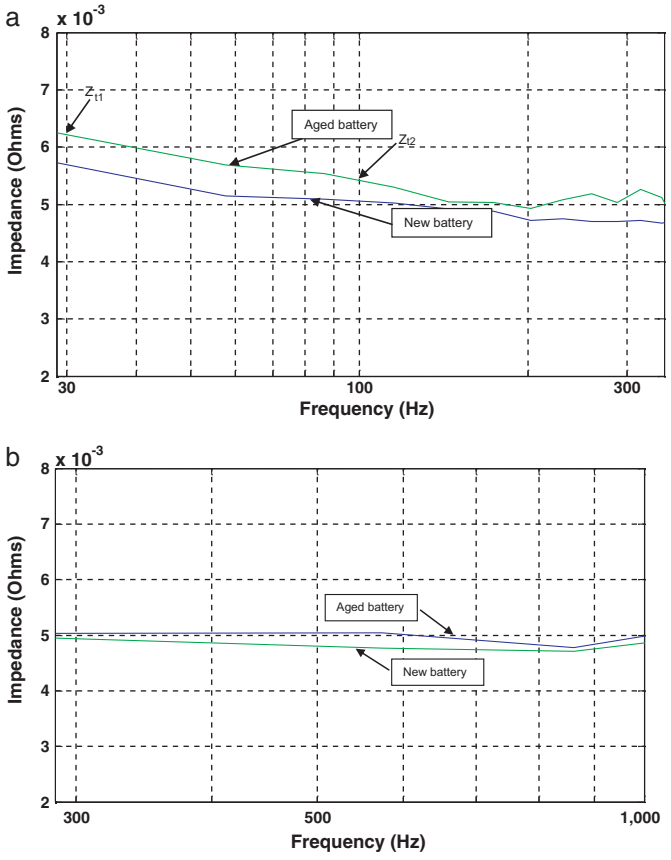

Fig. 14. (a) 30–300 Hz, impedance responses, showing effect of $C_{surface}$ and R_t in parallel, in series with R_i. Fig. 14 (b) 300–1000 Hz impedance responses showing response tending to the value of R_i.

the impedance of the parallel combination of R_t and $C_{surface}$ at these frequencies will be:

$$Z_1 = Z_{t1} - R_i \tag{18}$$

$$Z_2 = Z_{t2} - R_i \tag{19}$$

Substituting Z_1 and Z_2 into equation (17) and solving equation for $C_{surface}$:

$$C_{surface} = \sqrt{\frac{1/{Z_z}^z - 1/{Z_1}^z}{({\omega_2}^2 - {\omega_1}^z)}} \tag{20}$$

Fig. 14(a) and (b) below show responses from the batteries under test. Points taken from Fig. 14(a) at two frequency values, allowed C_s and R_t to be calculated in conjunction with Fig. 14(b) from which R_i was obtained.

6.3. Summary of results

The PRBS analysis of the two batteries yielded some interesting results in that the values obtained for R_i for the conventional and frequency domain tests were in the healthy range for both batteries (Table 2). This is interesting in that the aged battery was expected to be more obviously degraded, yet measurement of C_{bulk} revealed a reduction in rated capacity of only 7%. The value of $C_{surface}$ yielded the most information, the aged battery showing a considerable reduction in this value. Despite appearing relatively healthy this hinted at the underlying age of the battery and therefore a potential indicator of SoH.

To seek confirmation of the PRBS findings, further higher rate discharges were carried out which yielded information supporting

Table 2
Experimental PRBS results, pulse test results from Table 1 in parentheses.

New battery		Aged battery	
$C_{surface}$ = 16.4F	(14.81 F)	$C_{surface}$ = 4.54 F	(5.59 F)
R_i = 5.0 mΩ	(5.08 mΩ)	R_i = 5.05 mΩ	(5.6 mΩ)
R_t = 4.0 mΩ	(5.18 mΩ)	R_t = 4.24 mΩ	(6.5 mΩ)

the PRBS experiments. Discharge rates of $c/4$, $c/2$ and $1c$ were used, and the differences in capacity between the aged and new batteries increased. The tests indicated the aged battery tending towards 20% reduction in capacity at the $1c$ discharge rate, further indicating the degradation of the aged battery.

7. Conclusion

This paper has further demonstrated that a PRBS based monopolar current pulse load can be used in system identification for VRLA batteries, leading to the identification of specific battery parameters, particularly $C_{surface}$, R_i and R_t. The PRBS tests were successfully verified by the conventional tests, and comparisons to conventional current pulse methods show clear advantages of the technique. The parameters were identified with short duration tests, and when compared to spot frequency analysis a clear benefit was discovered with the aged battery. Commercial battery test equipment generally operates at singular frequencies in the 1 kHz range. At this frequency only R_i can be examined, and in the case of the test batteries the aged battery showed this value to be in a healthy range (as compared to the new battery). However, the value of $C_{surface}$ had reduced by a large margin, and C_{bulk}, although not measurable directly using the PRBS, was found to be reduced, albeit to a lesser extent. The change in $C_{surface}$ seen may be an early indicator of impending failure or catastrophic capacity loss. Additional discharge tests revealed that at increased discharge rate the capacity of the aged battery was further impacted, and this shift in the Peukert coefficient was indicated by the change in $C_{surface}$. Interestingly, the PRBS results generally gave lower impedance values than the pulse tests, and this could be attributed to a number of factors. The pulse tests required a steady state load to be applied for a period of time, leading to a small partial discharge of the battery. It is known that overall battery impedance can increase by 40%, between 100% SoC and 0% SoC [13], which may have contributed to the difference, and further justifies the non-intrusive nature of the PRBS technique. Furthermore, interpretation of the pulse test curves itself is difficult, in that the time constant (τ) is small when compared to the magnitude of the voltage deviations measured, leading to opportunities for errors in the resultant calculations. The PRBS technique is not subject to these issues, and it therefore follows that battery tests using PRBS should exhibit better accuracy than the conventional pulse tests. The observations made using the PRBS clearly indicate that the measured reduction in $C_{surface}$ is a SoH indicator for this battery. It is envisaged that further characterisation of a range of batteries would inform this correlation between $C_{surface}$ and SoH.

References

[1] K.S. Ng, C.-S. Moo, Y.-P. Chen, Y.-C. Hsieh, Applied Energy 86 (2009) 1506–1511.
[2] P. Bentley, et al., EPE2003, Toulouse, France, 2003.
[3] M. Coleman, W.G. Hurley, L. Chin Kwan, IEEE Transactions on Energy Conversion 23 (2008) 708–713.
[4] P. Mauracher, E. Karden, Journal of Power Sources 67 (2010) 69–84.
[5] B.S. Bhangu, P. Bentley, D.A. Stone, C.M. Bingham, Vehicle Power and Propulsion, 2005 IEEE Conference, 2005, p. 10 pp.
[6] A.J. Fairweather, M.P. Foster, D.A. Stone, IET Conference Publications, 2010, 2010, TU244.
[7] C. Tlili, H. Korri-Youssoufi, L. Ponsonnet, C. Martelet, N.J. Jaffrezic-Renault, Talanta 68 (2005) 131–137.
[8] S. Feliu, J.A. Gonzalez, C. Andrade, V. Feliu, Corrosion Science 26 (1986) 967–970, 961-965.
[9] H.J. Bergveld, W.S. Kruijt, P.H.L. Notten, Battery Management Systems: Design by Modelling, Kluwer Academic, Dordrecht; Boston, 2002.
[10] J.E. Randles, Faraday Discussions of the Chemical Society (1947) 11.
[11] D. Linden, Handbook of Batteries, 2nd ed., McGraw-Hill, New York, 1995.
[12] Yuasa NP Valve Regulated Lead Acid Battery Manual, Yuasa Battery Corporation, 1999.
[13] D. Linden, T.B. Reddy, Handbook of Batteries, 4th ed., McGraw-Hill, New York, 2010.
[14] B.S. Bhangu, P. Bentley, D.A. Stone, C.M. Bingham, IEEE Transactions on Vehicular Technology 54 (2005) 783–794.
[15] D.G. Jamieson, T. Schneider, Engineering in Medicine and Biology Magazine, IEEE 13 (1994) 249–254.
[16] T.J. Hamilton, A. van Schaik, B. Cornell, Biomedical Circuits and Systems Conference, 2008 (BioCAS), IEEE, 2008, pp. 361–364.
[17] M. Allain, P. Viarouge, F. Tourkhani, Canadian Conference on Electrical and Computer Engineering (2005) 574–577.
[18] W.D.T. Davies, System Identification for Self-adaptive Control, Wiley-Interscience, London, New York, 1970.
[19] R. Pintelon, J. Schoukens, System identification: a frequency domain approach, IEEE Press, New York, 2001.
[20] J. Schwarzenbach, K.F. Gill, in: E. Arnold (Ed.), System Modelling and Control, 2nd ed., 1984, London, Baltimore, Md.